MIT Open Access Articles

Label#Free Biophysical Markers from Whole Blood Microfluidic Immune Profiling Reveal Severe Immune Response Signatures

Massachusetts Institute of Technology

Label-free biophysical markers from whole blood microfluidic immune profiling reveals severe immune response signatures

Kerwin Kwek Zeming[1], Rohan Vernekar[2], Mui Teng Chua[3,4], Kai Yun Quek[1], Greg Sutton[2], Timm Krueger[2], Win Sen Kuan[3,4,] and Jongyoon Han[1,5,*]*

Dr. K. K. Zeming, K. Y. Quek, Prof. J. Han
[1]Singapore-MIT Alliance for Research and Technology (SMART) – Critical Analytics for Manufacturing of Personalized Medicine (CAMP) IRG
1 Create Way, Enterprise Wing, #04-13/14, Singapore 138602

Dr. R. Vernekar, G. Sutton, Dr. T. Krueger
[2]School of Engineering, Institute for Multiscale Thermofluids, University of Edinburgh, United Kingdom
Peter Guthrie Tait Road, Kings Buildings, Edinburgh EH9 3FD, United Kingdom

Dr. M. T. Chua, Dr. W. S. Kuan.
[3]Department of Surgery, Yong Loo Lin School of Medicine, National University of Singapore
1E Kent Ridge Road, Level 8, NUHS Tower Block, Singapore 119228

Dr. M. T. Chua, Dr. W. S. Kuan.
[4]Emergency Medicine Department, National University Hospital, National University Health System, Singapore
9 Lower Kent Ridge Road, Level 4, National University Centre for Oral Health, Singapore 119085

Prof. J. Han
[5]Department of Electrical Engineering and Computer Science & Department of Biological Engineering, Massachusetts Institute of Technology
77 Massachusetts Avenue, Room 36-841, Cambridge, MA 02139

*Correspondence email:
Prof Jongyoon Han, jyhan@mit.edu
Dr Win Sen Kuan, win_sen_kuan@nuhs.edu.sg

Keywords: immune profiling, deterministic lateral displacement, cell deformability, inflammation biomarkers, infection

Abstract

Disease manifestation and severity from acute infections are often due to hyper-aggressive host immune responses which changes within minutes. Current methods for early diagnosis of infections focus on detecting low abundance pathogens, which are time-consuming, of low sensitivity, and does not reflect the severity of the pathophysiology appropriately. The approach here focuses on profiling the rapidly changing host inflammatory response, which in its over-exuberant state, leads to sepsis and death. A 15-min label-free immune profiling assay from 20 μL of unprocessed blood using unconventional L and Inverse-L shaped pillars of deterministic lateral displacement (DLD) microfluidic technology was developed. The hydrodynamic interactions of deformable immune cells enable simultaneous sorting and immune response profiling in whole blood. Preliminary clinical study of 85 donors in emergency department with a spectrum of immune response states from healthy to severe inflammatory response shows correlation with biophysical markers of immune cell size, deformability, distribution, and cell counts. The speed of patient stratification demonstrated here has promising impact in deployable point-of-care systems for acute infections triage, risk management and resource allocation at emergency departments, where clinical manifestation of infections severity may not be clinically evident as compared to inpatients in the wards or intensive care units.

(200 words)

1. Introduction

The immune response is a dynamic system primed to resolve exogeneous or endogenous triggers such as cancers, infections, toxins, cardiovascular diseases, diabetes, *etc.* Despite advances in disease diagnostics, the main culprit for disease manifestation, severity and death is the hyper-aggressive host immune response in most instances.[1-3] In the example of severe COVID-19 infection, the leading cause of death is sepsis (dysregulated immune response) while existing risk stratification methods based on age and co-morbidity remains challenging and imprecise.[4, 5] The status of the patients' immune response can quickly change in a matter of minutes, therefore assays which are able to rapidly inform on the state of the immune system are vital in early triage among patients with acute infection, as well as prediction of downstream deterioration of disease.[6, 7] This enables delivery of appropriate medical response, particularly in the emergency department (ED), for timely intervention before immune dysregulation becomes clinically evident and requiring admission to the intensive care unit (ICU). Unlike patients in the ICU who almost always have clear clinical manifestations of disease severity and organ dysfunction (e.g. low blood pressure, decreased oxygenation, jaundice, low urine output), those in the ED frequently show non-specific symptoms and signs, which pose a challenge for physicians to assess the presence of infection and possibility of deterioration into organ dysfunction.

Current investigations for profiling the immune system and its activity include measurement of leukocytes gene expression, cell-surface biochemical markers and blood serum cytokine profile.[8-11] Recently, Bakr *et al.* showed a 'sample-sparing assay' where leukocytes can be extracted from small volumes of blood for immediate downstream tests of biochemical secretions and electrical properties [12]; Ellet *et al.* developed a neutrophil motility measurement to correlate sepsis in patients within ICU and heightened immune migration activity.[13] Toepfner *et al*. have develop label-free single cell immune morpho-rheological

analysis to detect human disease conditions related to immune response at 1000 cells/s.[14] Unfortunately, all these methods generally require sample dilution or pre-processing steps, as well as laborious, costly equipment and antibody labelling procedures. In most cases, returning results requires at least a few hours, which is a significant drawback in terms of their clinical utility for rapid triage and limit the implementation as routine practice within the emergency department or ICU. In addition, standard sample processing steps such as sample dilution, antibody labelling, and blood lysis centrifugation, could trigger changes in native immune cell activity which convolutes the immune profiling.[15-17]

In this study, we develop a rapid label-free immune profiling deterministic lateral displacement (DLD) assay as a quantitative diagnostic measure of immune cell biophysical signature using 20 µL of whole undiluted blood in under 15 mins. The assay is based on a simple workflow where whole blood is loaded onto a microfluidic chip and the DLD assay simultaneously sort immune cells (WBC) from whole blood and profile the biophysical properties of size, deformation, distribution and cell count which correlates to the immune states. Conventionally, DLD microfluidics has been used extensively as a sorting method for proteins, exosomes, DNA, red blood cells (RBCs) , white blood cells (WBCs), cancer cells and stem cells.[18-25] The deterministic nature of particle interactions within DLD devices result in predictable and high-resolution (~10 nm) sorting.[18, 26] Here, we discover that unconventional L and inverse-L (L^{-1}) DLD pillar structures interact and sort WBCs differently resulting in unique biophysical signatures. We translated the DLD precision sorting into an assay to quantify and profile the immune states of WBCs reflecting severity of immune response.

The biophysical DLD assay was performed directly on whole blood samples from healthy donors and patients recruited from the ED. Interestingly, the DLD assay reveals divergent biophysical signatures of immune cells from patients with infection versus immune cells

4

triggered *in vitro* with known activators such as lipopolysaccharides (LPS) and phorbol 12-myristate 13-acetate (PMA). These findings suggest *in vitro* immune cell activation do not mimic physiological immune cell response and emphasize the significance of this work on profiling immune cells in its native physiological state – whole blood with minimal
5   perturbation.

We further evaluated the diagnostic modality by recruiting 8 healthy donors, 36 donors with non-infection symptoms such as cardiac conditions and 41 donors presenting to the ED with 2 or more components of the systemic inflammatory response syndrome (SIRS) [27]. The
10   DLD assay on a single drop of blood reveals significant immune biophysical response signatures which resulted in distinction between infection and non-infection group with a detection sensitivity of 0.91 and specificity of 0.92.

With a whole blood sample throughput of up to 10,000 cells/s using video captured frame
15   rates of 15 to 150 fps, we showed that our biophysical diagnostic modality can be easily achieved using low-cost and compact machine vision cameras or smart phone optical sensors making it attractive for deployable point-of-care systems for rapid patient triage of immune dysregulation in ED. This could potentially change disease diagnosis, treatment, and risk management in the settings of primary care and hospitals.

20

2. Results

2.1 WBC biophysical measurements in DLD device

The DLD devices used for immune cell profiling assay consist of a polydimethylsiloxane (PDMS) device with three open reservoirs and a single outlet tubing attached to a syringe pump (**Figure 1a**). The open reservoirs facilitate easy sample loading, sample resuspension to prevent settling of cells and washing the reservoir to reuse the device. The required loaded volume per run is 10 µL and the reservoir can hold up to 25 µL of blood. As the fluid is withdrawn, the sample flows through 21 DLD device segments sandwiched between two 1x phosphate-buffered saline (PBS) buffer streams (see Table S1). Each segment has a specific DLD critical cut-off size (D_c) determined by the empirical Equation 1.[28]

$$D_c = 1.4G tan\theta^{0.48} \tag{1}$$

where G is the regular spacing between pillars and θ is the gradient of the pillar array. This design is commonly known as a chirped DLD array where each downstream segment has an increasing pillar row-shift gradient corresponding to an increasing D_c ranging from 6.0 to 16.0 µm in steps of 0.5 µm (see Methods).[28] Immune cells flowing through the device are deflected laterally only within DLD segments where cell sizes are larger than D_c; the cells therefore exit the device at defined lateral positions depicted in the output region in Figure 1a (See Supplementary Video S1). The output of the sorting forms a spectrum in its size distribution. The apparent cell size (D_{app}) is the size that is exhibited in a DLD microfluidic device given the design parameters D_c from Eq (1) and the observed outlet distribution.

The DLD assay has a minimum measurable D_{app} of 6.0 µm, and RBCs having an apparent size of less than 3.0 µm would not be deflected laterally in the DLD device. As such, the input and output lateral position of RBCs remains the same, albeit with a larger spread at the outlet region. This spread is due to diffusive effects and the stochastic nature of RBC

interaction within the DLD (Figure 1a). The distribution of WBCs across the outlet can be counted and analysed for its apparent mean size and standard deviation (S.D.).

Two DLD pillar structures were investigated in this study, namely L and L^{-1} (Figure 1b and Supplementary Figure S1). Previous studies have shown contrasting sorting effects of these two pillars on the highly deformable and biconcave disc-shaped RBC.[29] Despite the preliminary evidence of size and shape deformability sorting of RBCs, information on DLD pillar shape effects on generally spherical and deformable WBCs is lacking. In this work, we aim to utilize the unique WBC sorting signatures of these different DLD pillar structures as an assay to profile the activation state of WBCs (Figure 1b). By using different flow velocities, each DLD assay elicits a unique biophysical interaction with deformable WBCs. These biophysical traits and parameters are aggregated and used to classify the WBC state as activated or non-activated.
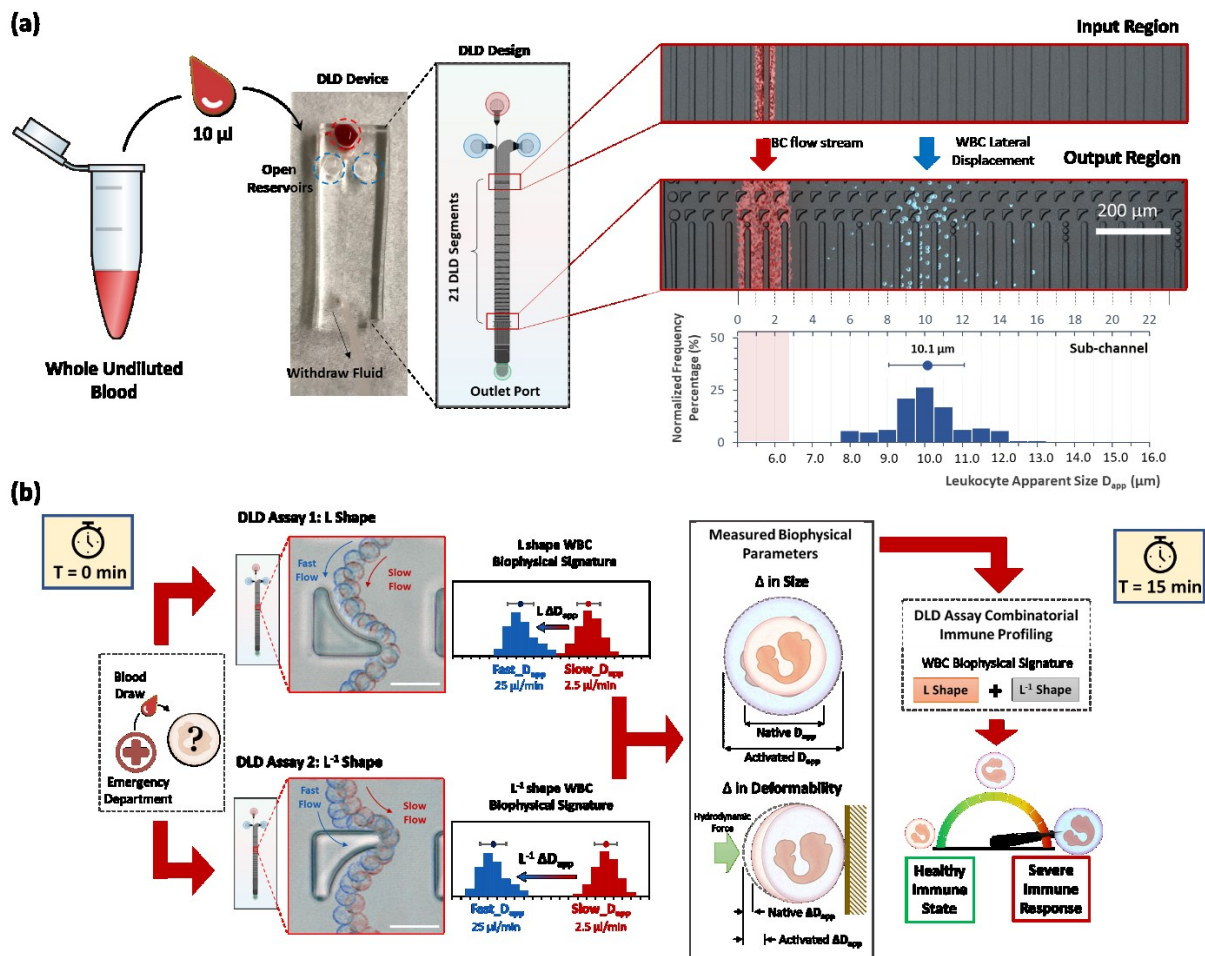
Figure 1. Schematics of experiment and immune profiling workflow using DLD assays for L and L^{-1} pillar shapes. (a) shows the whole blood DLD assay by loading the blood into the sample reservoirs of the PDMS DLD device which is used to simultaneously sort and measure the distribution of cells across the output region allowing size frequency distribution analysis (See Supplementary Video S1). The device consists of two additional buffer reservoirs which sandwich the sample stream resulting in a precise injection of sample into the DLD region. The DLD region is composed of 21 DLD segments corresponding to 21 step measurement resolution ranging from size 6.0 to 16.0 µm in steps of 0.5 µm. The streams in input and output regions are in pseudo-colour to show the differences between input and output. Scale bar is 200 µm. (b) describes the DLD assay(s) used to profile WBC based on their unique biophysical signatures in the different DLD pillar structures. These biophysical parameters are used to then classify the immune spectrum from healthy to severe immune response.

2.2 Effect of Flow Rates on WBC Size and Deformation

WBCs are deformable particles and their morphology changes with application of external forces. The D_{app} of WBCs decreases as fluid flow rate increases (**Figure 2a-b** and see

Supplementary Video S2). For the L-shaped DLD assay, the WBC output spectrum shows a mean D_{app} of 9.7 µm, 9.3 µm, 8.2 µm and 7.7 µm for flow rates of 2.5, 5.0, 10.0 and 25.0 µL/min, respectively. In the L^{-1} DLD device, WBCs have mean D_{app} from 10.1 µm, 9.5 µm, 8.6 µm to 7.1 µm. The reduction in mean D_{app} at 2.5 µL/min to 25 µL/min is denoted by

5   ΔD_{app}, which corresponds to L ΔD_{app} = 2.0 µm and L^{-1} ΔD_{app} = 3.0 µm. This measures up to at least 15% reduction in mean D_{app} as the flow rate increases.

The difference between two DLD assays using the same sample can be interpreted clearer in the graph plot in Figure 2c where D_{app} is plotted against flow velocity. The trend is linear in the logarithmic scale, resulting in a log-linear equation measuring the change of D_{app} with

10   respect to fluid flow velocity. We define the modulus of the gradient as DLD cell-deformability modulus (CDM). The CDM parameter quantifies the change in WBC apparent size over varying flow velocities from the measurement at 2.5 µL/min. The CDM parameter for   L   and L^{-1} are denoted as CDM_L and CDM_{L-1}, respectively. As the L DLD assay showed a smaller L

15   ΔD_{app}, the CDM_L is correspondingly smaller at 0.94 as compared to CDM_{L-1} at 1.31.

DLD profiling assays using L and L^{-1} pillar shapes lead to different sorting signatures for deformable cells. On the contrary, the same DLD assay performed on rigid beads shows no significant change in D_{app} at different flow rates for L and L^{-1} DLD tests (Supplementary Discussion 1 and Figure S2). This strongly demonstrates that unequal cell deformation results

20   in different flow outcomes in L and L^{-1} DLD pillar structures.
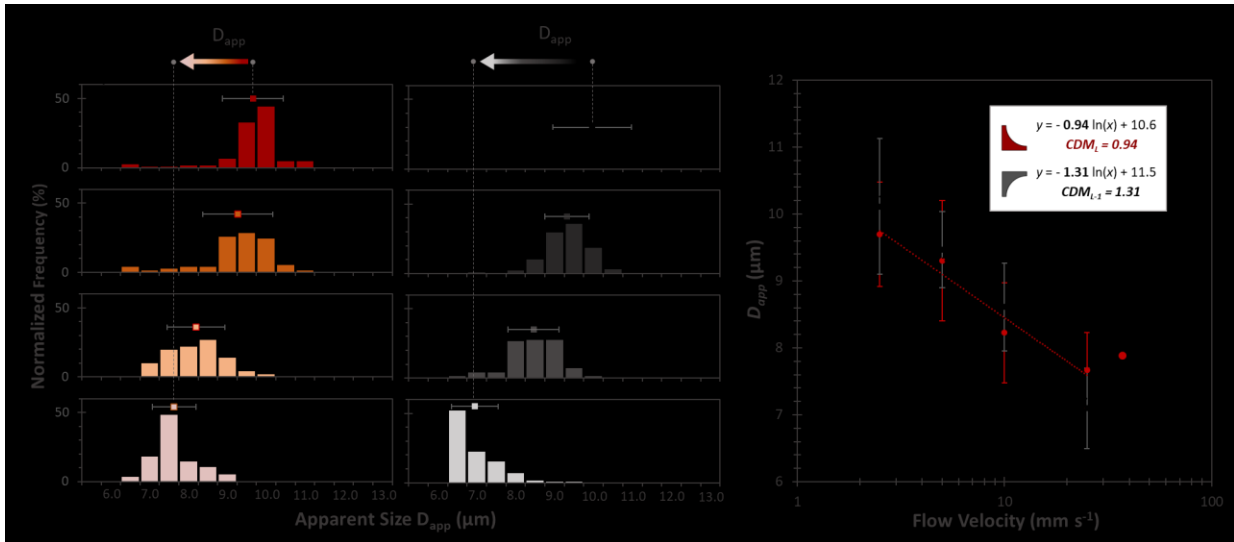
Figure 2. Size and deformability measurements of WBCs in L and L^{-1} DLD devices. The frequency distribution plot for the measure D_{app} of WBCs at various flow velocities in different devices are shown in (a) for L and in (b) for L^{-1}. The L ΔD_{app} and L^{-1} ΔD_{app} were measured at 2.0 and 3.0 µm, respectively. n > 100 were used for each distribution and the error bar denotes the sample standard deviation. (c) introduces the cell DLD-deformability modulus (CDM) parameter where the rate of change of size can be measured by plotting the fitting equations of the size plots for L and L^{-1}.

2.3 Visualizing WBC flow signatures in DLD assays

In the DLD assay, measured D_{app} varies depending on the pillar structure. This is primarily due to WBC deformability, resulting in differences in their periodic flow trajectories as they navigate between the two consecutive DLD pillar micro-structures. The simulated hydrodynamic streamlines visualize the fluid motion with respect to the cell (**Figure 3a** and 3b), clearly showing fluid flow differences. This principle becomes clearer when the experimental cell trajectory is tracked within a small DLD pillar unit for L and L^{-1} structure (Figure 3c and 3d, darker false colour). Each pillar structure interacts with the deformable cell in complex ways, and it is evident that the paths taken by cells at slow ($Q_1 = 2.5$ µL/min) and fast ($Q_2 = 25.0$ µL/min) flow rates differ between L and L^{-1} DLD pillars. DLD relies on repetitive interactions between stationary pillars and moving cells, any small difference in

cell path over a single pillar accumulates and the sum-total of all pillar interactions translates to a larger sensible change in D_{app} measured at the output of the DLD devices.

In total, four resolved 2D flow-coupled cell simulations were performed at flow rates of Q_1 and Q_2, in both the L and L^{-1} DLD periodic geometries (Supplementary Methods 1 and Supplementary Discussion 2). The results of the simulated WBC trajectories are overlaid on the experimental pillar structure in Figures 3e and 3f. The general trends seen in the experiments are well captured in the simulations. As the cells experience larger shear gradients nearer the pillar walls, the spherical WBCs are pinched into a "kidney-bean" shape at higher flow rate Q_2, as seen in both experiments and simulations (Supplementary Video S3 and S4). This cell deformation at increasing fluid flow rates is the leading cause of the decreasing D_{app}.

Detailed analyses of simulated WBC velocity for each pillar structure provide a deeper understanding of cell-DLD interactions (Figure 3g - 3j and Supplementary Figure S3, S4 and S5). The simulated cell velocities V_1 and V_2 (corresponding to Q_1 and Q_2 flow rates, respectively) are plotted for L and L^{-1} (Figure 3g and 3h). For L DLD pillars, the V_2 profile largely matches that of V_1, demonstrating that deformability-induced trajectory changes, if any, are rather minor. In contrast, L^{-1} DLD pillars show that V_2 and V_1 (resulting from high and low flow rates) are quite dissimilar, demonstrating a significant deformability-induced effect on cell velocity and trajectory. Specifically, V_2 drops closer to zero than V_1 when the cell collides with L^{-1} DLD pillars. In DLD, a particle velocity close to zero indicates a stagnation point, where the particle's D_{app} is close to the design D_c, therefore more likely to choose a zigzag pathway as smaller cells would.

The flow signature of the WBC flow mechanics imposed by the two pillar shapes is reflected in the ratio of cell velocity V_2/V_1 (Figure 3i and 3j and Supplementary Figure S6 and S7).

Since the particle Reynolds number is smaller than 1, Stokes flow dictates that hydrodynamic forces and velocities are linearly related, and thus our assertion that the velocity ratio for a rigid bead (whose dimensions remain the same with increasing flowrates) should give a constant that equals V_2/V_1, a value of 10 in the simulation. For the (deformable) WBCs, however, this constant scale-up will no longer hold, as the cell boundaries deform differently with increased flow rates. The L^{-1} velocity ratio shows a much greater reduction relative to the ideal rigid bead (Figure 3j).

From both simulation and experimental data, it is clear that L and L^{-1} have significant 'fingerprint' differences in inducing WBC deformation in the DLD assays, leading to the observed deviations in sorting behaviour. The L^{-1} shape pillar results in more significant reductions in velocity (and apparent cell size D_{app}) than the L shape. This is the theoretical basis to treat L ΔD_{app} and L^{-1} ΔD_{app} as the indicators of cell deformability.
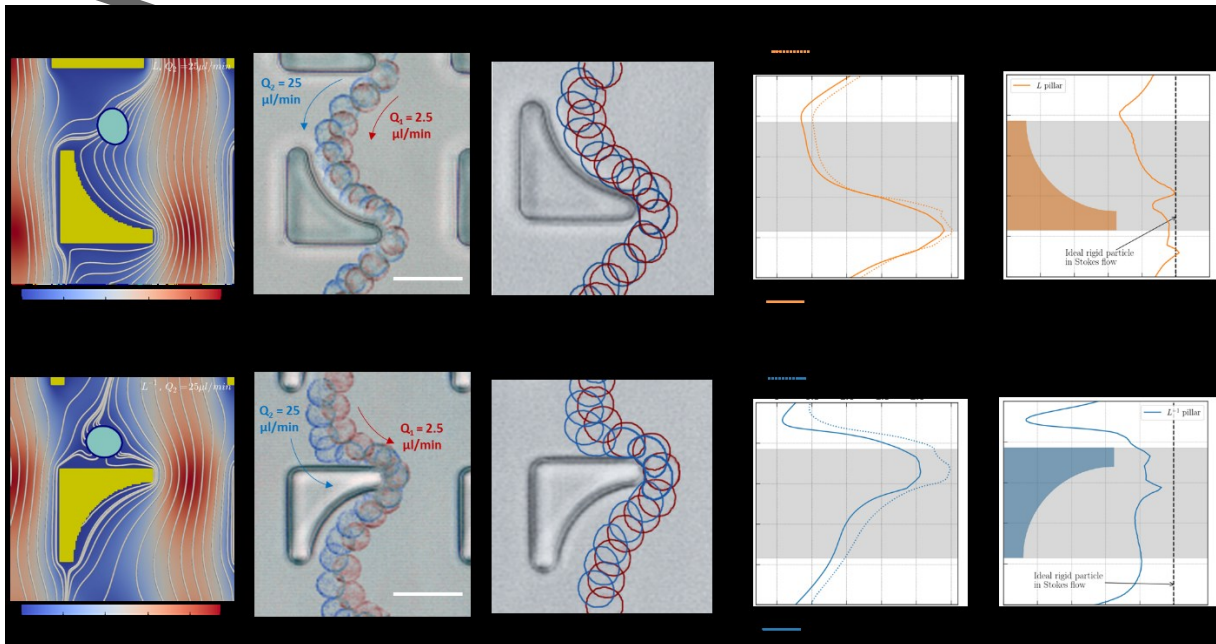
Figure 3: WBC paths over L^{-1} and L pillars and their simulated velocity signature. (a) and (b) shows the instantaneous simulated flow streamlines around a deformed WBC and DLD pillars. Magnified experimental time-lapse overlay of individual WBC trajectories and dynamics over L and L^{-1} structures is seen in (c) and (d), respectively. The colours dark blue and dark red are pseudo-colours highlighting experimental WBC sequential motion at two flow rates, $Q_1 = 2.5$ μL/min and $Q_2 = 25.0$ μL/min. Similarly, simulated motion of the 2D

WBC overlaid over the experimental DLD pillar images is seen in (e) and (f), with red and blue outlines depicting simulated flow at 2.5 µL/min and 25.0 µL/min respectively. (g) and (h) plot the simulated deformable cell velocity for slow flow (V_1, top axis) and fast flow (V_2, bottom axis) against flow-wise cell centre position (left axis) over single L and L^{-1} inverse pillars (grey region). (i) and (j) plots the dimensionless velocity ratio V_2/V_1 (bottom axis) against the same flow-wise cell position (left axis) over single L and L^{-1} pillars. This ratio displays two distinct 'fingerprint' signatures for the in the L and L^{-1} setups. The dashed line plots the theoretical limit for V_2/V_1 in Stokes flow regime for a rigid non-deformable particle for the tested Q_1 and Q_2 in both setups. Scale bar in (c) and (d) shows 20 µm.

2.4 WBC Biophysical Signatures in DLD Assay

Unlike rigid beads, the WBC sorting differences for L and L^{-1} DLD assays give rise to unique biophysical signatures, which we hypothesize can be utilized to profile WBC samples. To investigate the variations of the biophysical signature, the DLD assays were performed at the same flow parameters on 5 healthy donor samples shown in **Figures 4a** and 4b. L^{-1} D_{app} measures consistently higher at 9.98 ± 0.15 µm than L D_{app} at 9.37 ± 0.21 µm at 2.5 µL/min with a p-value of 0.004. The CDM measurements for the 5 healthy samples also showed consistent differences with CDM_{L-1} having a larger value of 1.19 ± 0.13 compared to CDM_L of 0.85 ± 0.07 with a p-value of <0.001. Both tests were performed using a paired 2-tailed *t*-test.

To evaluate the biophysical combinatorial immune profiling potential of DLD assay, a single biophysical size and deformability parameter is determined. For size parameters, the average D_{app} for L and L^{-1} assays was quantified at 2.5 µL/min, while a single cell deformability parameter (CDM_{dot}) was emphasized by taking the product of the CDM_L and CDM_{L-1} measurements. Performing a product amplifies the deformability differences compared to CDM_L and CDM_{L-1} measurements individually (See Supplementary Figure S8). By combining the measurements of two DLD devices, we envision a unique leukocyte

biophysical fingerprint as a profiling tool to measure different states of WBC from whole blood in real-time (Figure 1b).

2.5 DLD Assay Combinatorial Immune Profiling

Using the two parameters of D_{app} and CDM_{dot}, we profiled various conditions of immune cells from whole blood. Three groups of immune cell conditions were measured, namely direct sample sparing measurements, *in vitro* WBC assays and impact of blood processing methods on immune cell biophysical properties (Figure 4c).

Direct sample measurements enable the study of WBC biophysical profiles in different health states of an individual for healthy donors, patients admitted to the ED without signs of infection (ED Control), and patients with clear signs of infection and fulfilling at least two SIRS criteria (ED ≥2 SIRS) (See Supplementary Table S2). The second group highlighted in blue are tests performed on blood, which have undergone external or *in vitro* test conditions to activate the WBCs. These include 5 ng/mL lipopolysaccharide (LPS)[30], which mimics the bacteria coat that would trigger inflammation and phorbol 12-myristate 13-acetate (PMA) at 100 and 1000 nM, a known activator of WBCs. Lastly, standard blood processing methods were tested, specifically the commonly used RBC lysis protocol to retrieve immune cells and whole blood stored on ice. All tests were initiated within 1 hr of blood draw to accommodate the transport time of blood from hospital to laboratory and concluded within 15 mins of biophysical profiling.

The dotted line in Figure 4d denotes the baseline mean measurement of D_{app} for 5 healthy samples at 9.7 ± 0.1 μm. In comparison, for all tested conditions, WBC D_{app} only seems to increase and not decrease with varying magnitude for different conditions. For the closest *in vivo* model of direct sample injection, ED ≥2 SIRS showed a larger size of 10.4 ± 0.4 μm compared to ED control (9.8 ± 0.3 μm). In contrast, WBC biochemical activation with

14

incubation of PMA at 100 nM and 1000 nM for 2 hours showed a much larger increase of D_{app} at 12.6 ± 0.8 μm and 13.9 ± 0.7 μm, respectively. This is a drastic 30% to 43% increase in WBC D_{app}. Interestingly, the RBC lysis process also showed an increase in WBC D_{app}, which suggests potential activation and biophysical changes in the WBCs. Blood processing protocol to store blood samples on ice did not change the WBC D_{app}.

CDM$_{dot}$ measurements on the other hand describe a different parameter of the WBC. A larger CDM$_{dot}$ relative to the healthy donor measurements in Figure 4e indicates an increase in deformability while a reduced CDM$_{dot}$ shows a decrease in deformability. These CDM differences are benchmarked against the control measurements of healthy samples with a CDM$_{dot}$ of 0.98. A surprising result emerged from the deformability parameter measurement as all *in vitro* assays and sample pre-processing steps resulted in reduced deformation of WBC measured. This means that the size compression of WBC is reduced compared to the healthy baseline. On the contrary, direct sample injection tests showed that the WBC deformability increased instead when infection is present in the patient. The greatest change in deformability was demonstrated in samples of blood on ice where the CDM$_{dot}$ is greatly reduced to less than 0.10 while its size measurements did not change. The cold temperatures experienced by cells could potentially affect mechanical properties of cells due to stiffening of cytoskeletal networks[31-33] and lipid bilayer[34].
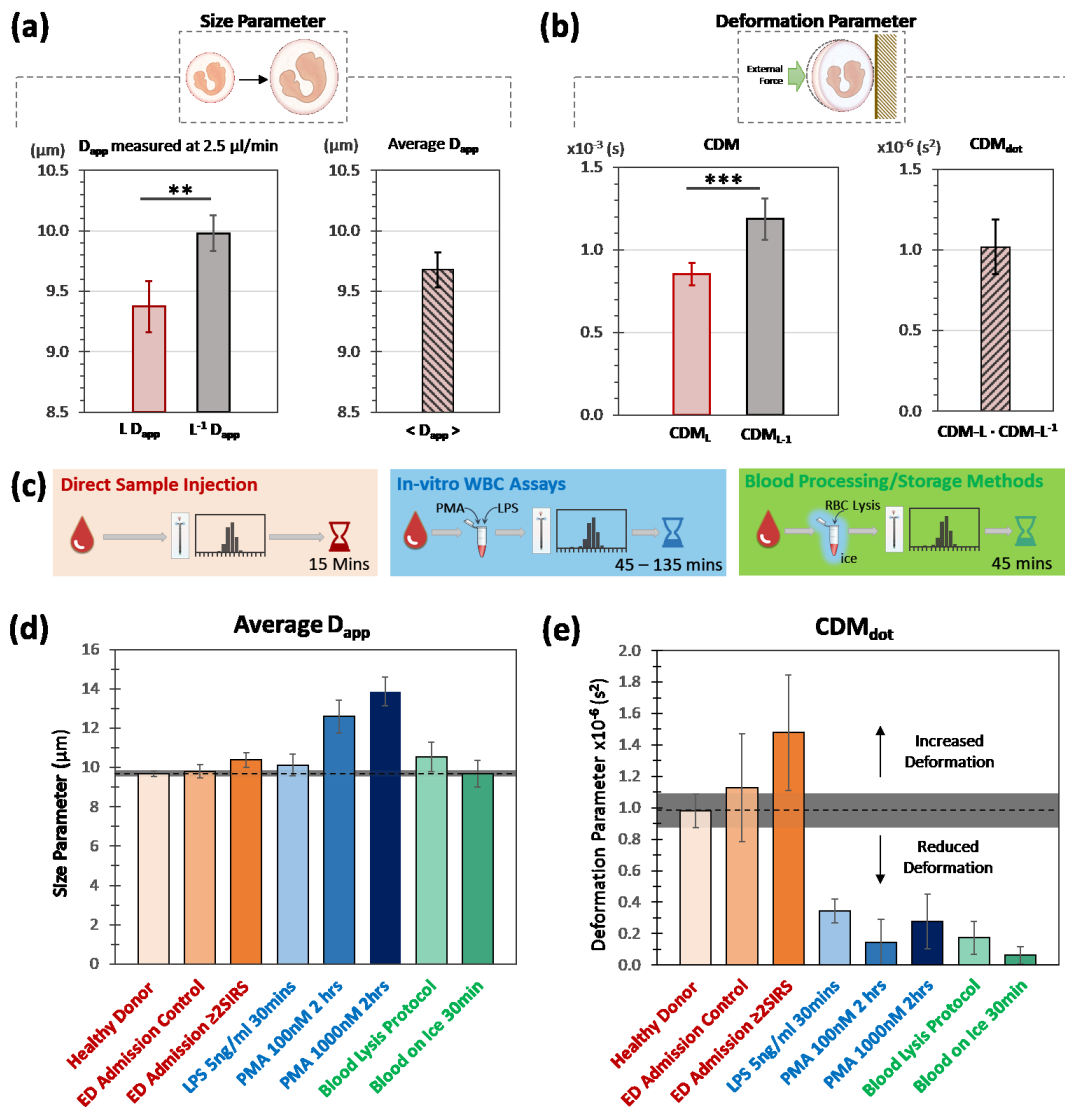
Figure 4: DLD Assay for WBC biophysical measurements of size and deformability from whole blood. n = 5 healthy donor samples were used to measure the size parameters in (a) and deformation parameters (b). D_{app} were measured at 2.5 µL/min for L and L^{-1} and a paired t-test with ** denoting p = 0.004. Average D_{app} is the mean of both L and L^{-1} where n = 5 and error bar denotes standard deviation of sample. The CDM deformation parameter for L and L^{-1} were plotted in (b) with *** denoting a p < 0.001 for a paired t-test of n = 5 sample. CDM_{dot} is the product of both CDM_L and CDM_{L-1}. (c) shows three groups of measurements performed, namely biophysical profiling of WBCs from direct sample injection (red), *in vitro* WBC assays (blue) and common blood processing/storage methods (green). Direct sample injections include a healthy donor control sample, emergency department (ED) admission control (i.e. patients with no clear signs of infection) and ED admission with infection and two or more SIRS criteria. The mean size measurement, D_{app}, across all samples are depicted in (d) while the deformability parameter CDM_{dot} is shown in (e). The horizontal dotted line denotes the mean value of healthy donor in (c) and (d) with standard deviation shown in the

gray region. n = 5 samples were used for all plots with standard deviation represented by the error bar.

WBCs from patients who have infections show an increase in deformation relative to WBCs of healthy donors. The divergence of CDM_{dot} measurements was unexpected. This suggest that *in vitro* assays mimicking WBC activation could not replicate the physiological conditions of WBC biophysical parameters despite incubation in whole blood at $37^{o}C$, as post-blood draw WBC activation assays illicit a different biophysical response relative to innate blood from infected patients. This evidently shows that activation of WBC is multi-dimensional and complex physiologically. Simple and single triggers of activation are highly unlikely the cause for the observed WBC biophysical characteristics. The data also emphasize the conflicting results of earlier studies showing WBCs of ICU sepsis patients being less deformable while works of Di Carlo *et al.* showed increase in WBC deformability during infection [35]. Ellett *et al.* also attempted to mimic sepsis via biochemical trigger cocktails but were unable to do so [13]. This highlights the importance of our current work in developing tools to probe innate immune states with minimal sample handling and *ex vivo* delay time.

2.6 Biophysical Immune Markers of Severe Inflammation

Patient recruitment from the ED of the National University Hospital, Singapore, was conducted with ethics approval from the local institutional review board (National Healthcare Group Singapore, Domain Specific Review Board, DSRB reference number: 2018/00115). Written informed consent was obtained from enrolled participants. Based on the results from Figure 4, we expanded the direct sample injection tests and recruited 85 donors comprising two broad categories of donors without infection or with infection. The "no infection" group includes 8 healthy donors (Healthy) and 36 ED admission controls (Controls) while the

"infection" group comprised 41 ED admissions with infection plus ≥2 SIRS criteria (see Supplementary Table S3). Additionally, instead of just size and deformability parameters, we evaluated cell count and the WBC distribution with a range of 38 identified biophysical markers parameters (features) listed from the DLD assay resulting in a clearly distinct PCA plot (See Supplementary Figure S9 and Supplementary Table S4 and Table S5).
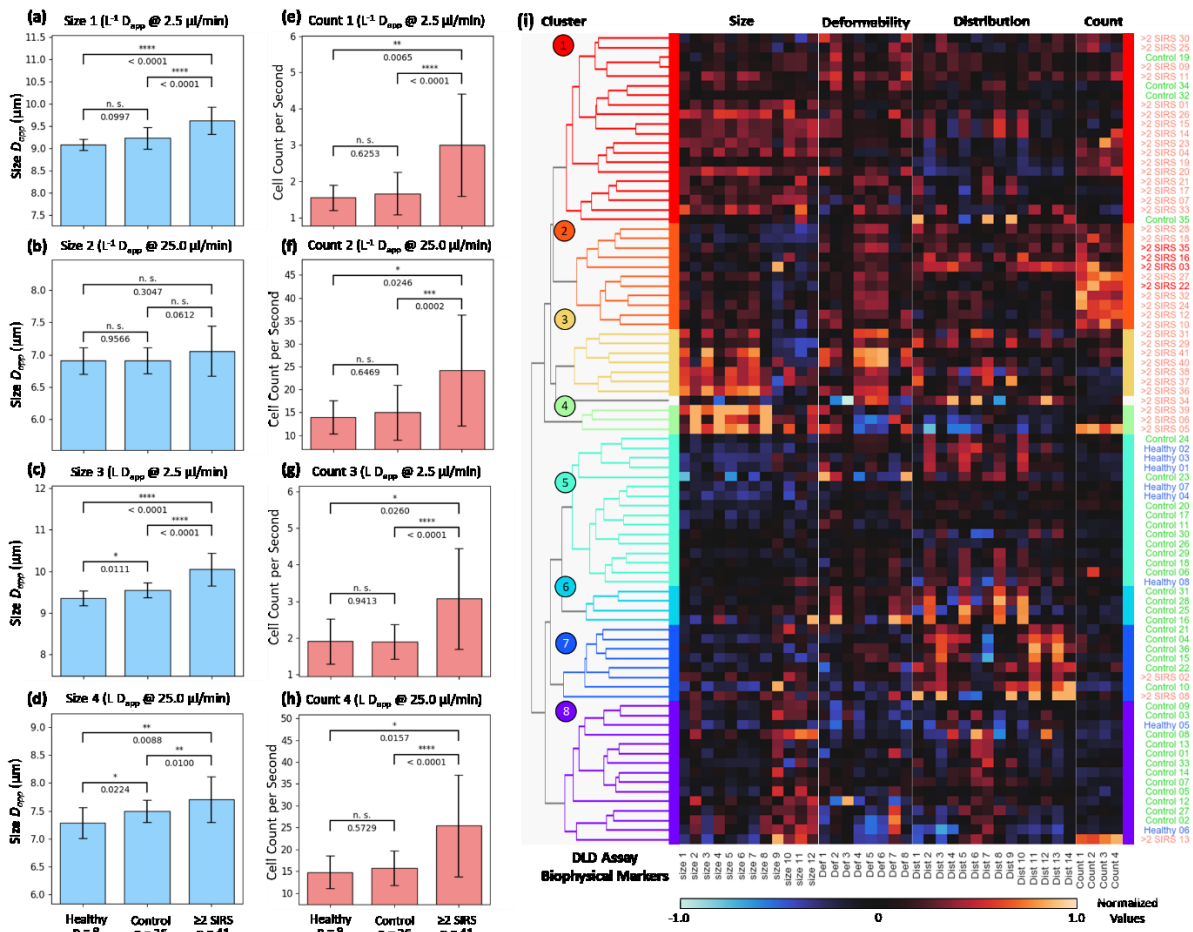
Figure 5. Comparing label-free biophysical immune markers and signatures of various immune status. (a)-(d) show plots for Size 1 to Size 4 features, while (e)–(h) show plots for cell Count 1 – Count 4, respectively from a list of 38 biophysical markers (See Supplementary Table S4). The plots compare the mean and sample standard deviation for healthy (n = 8) samples, Control (n = 36) samples and ≥2 SIRS (n = 41) samples. An independent two tailed t-test is used to compute the p-values of the sample measurements with n.s. denoting not significant, * for $p < 0.05$, ** for $p < 0.01$, *** for $p < 0.001$ and **** for $p < 0.0001$. (i) shows the hierarchical clustering and heatmap of normalized biophysical marker value of all 85 samples comprising healthy (green), no infection control (blue), infection tests >2 SIRS (pink) and severe immune response with >2 SIRS (red). 8 clusters were identified based on the data and the heatmap shows the corresponding biomarker

signatures. The biomarkers are grouped based on size, deformability, distribution and cell count.

By plotting the correlation heat map for all the biomarkers, we can distinguish between the various correlation clusters of the biomarkers. We performed the 2-tailed *t*-test shown in **Figure 5a-h** and Supplementary Table S4. Interestingly, we found that the L DLD assay in Figure 5c and 5d could significantly detect differences between all three inter-sample groups (sub-class) of healthy, control and ≥2 SIRS. Cell count data only showed distinct differences between control and ≥2 SIRS group. This is not unexpected as cell count is a parameter to assess SIRS criteria. However, it is highly intriguing that cell size (specifically L pillar in Size 3 and Size 4) were able to differentiate healthy from ED control group. This suggests that despite no clear signs of infection, the immune size is modulated based on medical conditions that the patients were admitted for. The mean cell size difference between the three groups range from 9 to 10 μm which validates the resolution of DLD assay to probe cells within this narrow D_{app} band. The corresponding statistical analysis for the deformability and distribution markers also showed significant distinction between no-infection and infection group (see Supplementary Table S4). The correlation heatmap shows that these markers are independently significant as they are not strongly correlated and can be used for immune profiling (see Supplementary Figure S10).

We tabulate the 38 biophysical markers of all tested samples and performed hierarchical clustering based on the DLD assay biophysical markers (Figure 5i). The unsupervised clustering grouped the data into 8 clusters with visible biophysical signatures and profiles. Patients with >2 SIRS were generally clustered in group 1 – 4 while non-infection control and healthy donors were grouped in cluster 5 – 8. Visible distinction between these groups can be seen in the heatmap. Size and deformability-based biomarkers were elevated for >2 SIRS group while cell distribution biomarkers levels were cluster specific. Cell count

biomarker were only highly expressed in certain samples and is not directly correlated with size-based markers for group 3 and 4. This suggest that biophysical markers such as immune cell size and deformability is potentially more sensitive to profile the immune activation states than lagging changes in cell count.

5   Interestingly, 4 patients from >2 SIRS group were later diagnosed to have sepsis with a SOFA score of >4 identified by red labels for >2 SIRS 03, 16, 22 and 35 in Figure 5i and were grouped in cluster 2. These group showed moderate increase in size and cell count but relatively larger increase in cell deformability and distribution markers. Cluster group 2 also correlated a longer hospitalization stay and this biophysical signature could be useful to

10   prognose severity of disease progression and risk of hospitalisation (See Supplementary Figure S11).

>2 SIRS 02, 08 and 13 immune signatures were clustered in group 5 – 8 which was predominantly healthy and non-infection controls. This clustering independently shows that these patients, though exhibiting >2 SIRS, had a lower immune response signature profile

15   which resulted in a short hospitalisation stay of only 1-2 days. On the contrary, Control sample 19 in cluster 1 had a relatively longer hospitalisation stay of 10 days.

Finally, the predictive value of 38 biophysical markers to classify non-infection versus infection class of 85 patient samples was analysed using the receiver operating characteristic (ROC) curve in Figure S12 and S13. The area under curve (AUC), specificity and sensitivity

20   of the assay was 0.97, 0.91 and 0.92 respectively. This result was performed based on support vector machine model for classification (Figure S13)

3. Discussion

The DLD devices function as sensitive and quantitative assay of immune cell biophysical signatures in relation to the WBCs' real-time activation levels. The swift response of the immune system induced by biochemical triggers are also expressed in biophysical properties of the leukocytes for effective extravasation and other functions.[13, 36] Studies have shown correlation of immune cell biophysical changes with cytoskeletal remodelling, protein production and cell proliferation.[37-39] As WBCs are activated by various internal or external triggers, the extent and direction of these changes were sensitively measured using the DLD assay explored in this manuscript. This work highlights new insights, which advances both engineering of precision microfluidics and clinical research.

First, various DLD structures were shown to illicit different sorting signatures on deformable cells. The selection of L and L^{-1} was not arbitrary as it is based on previous observations on RBC sorting performance.[29] What it entails here is also the possibility that more suitable DLD pillar shapes can exist for the function of biophysical DLD assays. To uncover potentially useful DLD shapes requires deeper and fundamental understanding of particle-pillar-fluid interactions, especially for deformable particles. Our empirical evidence and simulations show that using these different signatures, we can define a collective cell D_{app} and deformability response that quantitatively predicts a cell state.

Second, the WBC biophysical DLD assay showed divergent deformability response for *in vitro* assays and direct whole blood assay. *In vitro* assays here, which aim to study WBC immune response, were not able to replicate the biophysical deformability properties of WBC from patients who show clear signs of infection. This could be due to blood treatment methods using ethylenediaminetetraacetic acid (EDTA), stimulants concentration and incubation time.[30, 40] Recent advances in microfluidic devices based on high-throughput single cell deformability imaging cytometry mechano-phenotyping also showed that natively

activated immune cells increases its deformability and size and also showed oscillating immune activity during immune activation and sepsis.[14, 41-43] Similarly, our work based on whole blood rapid immune profiling supports this crucial finding and raises new research questions and potentially challenging current methods of using *in vitro* studies to elucidate physiological immune responses.

Finally, the clinical study shows that patient classification using DLD biophysical assay was possible showing distinct label-free biomarker profiles of healthy donors and patients admitted to the emergency department with and without infection. Our approach differs substantially from previous ICU-based studies where patients who have clear manifestations of symptoms and signs of severe disease and immune dysregulation.[44] Importantly, these patients were recruited at admission to the ED with diverse pre-existing conditions such as diabetes mellitus and hypertension but did not progress to full-blown sepsis, characterized by presence of organ dysfunction. Yet, immune biophysical markers show independent and good indication of its diagnostic or prognostic potential, especially the possibility for identifying patients with non-infection-related medical conditions. While a larger clinical study is needed to further evaluate potential biophysical immune response phenotypes and the its utility in the field, our study adds scientific evidence to existing works on biophysical parameters as an important marker for immune profiling.[45]

4. Conclusion

This paper studies the unique biophysical signatures when immune cells are sorted from whole blood within unconventional DLD pillars of L and L^{-1} shape. These signatures result in the formulation of 38 biophysical markers which enable the profiling of immune responses of patients recruited from emergency department with a detection sensitivity of 0.91 and specificity of 0.92. Given that the DLD assay takes 15 minutes to perform, uses less than 20

μL of whole blood and only requires video capture frame rates of up to 150 fps, the system can potentially be developed into a portable unit for point-of-care whole blood sparing assays which could significantly improve the diagnosis and stratification of patients with systemic inflammation response syndrome within the ED and other primary care settings. The

5   availability of such an adjunct with both real-time information and rapid turnaround time is crucial as incoming patients to the ED from the community are highly undifferentiated. Being able to quickly identify at-risk patients and render measures to prevent organ dysfunction will be the key actionable information provided by this tool. This contrasts with patients in the ICU who already have clinical evidence of organ dysfunction through standard laboratory

10 investigations and physiological parameters.

5. Experimental Section/Methods

5.1 Device Design

DLD is a sensitive size-based sorting technique, using a regularly spaced pillar array where the separation can be determined by the established empirical formula: [20]

$$D_c = 1.4G \tan\theta^{0.48} \qquad (1)$$

Where G is the regular spacing between pillars and θ is the offsetting angle of the pillars. We designed two DLD chips with 21 DLD segments to compare L and L-1 shape DLD pillars. The G used here measures 23 μm and with D_c of device ranging from 6.0 to 16.0 μm, each DLD segment increases the D_c by a step of 0.5 μm. The period of the array is 50 μm.

5.2 Device fabrication

The device was fabricated using standard photolithography methods. A chromed quartz mask with the designs specified was ordered from JD Photo Data (Hitchin, UK). A mask aligner was used to fabricate an SU-8 mold using SU-8 2015 and spun to a thickness of approximately 20 μm. Poly-dimethylsiloxane (PDMS) (Dow Corning, Midland, Michigan) was added in a ratio of 1:10 and poured onto the SU-8 master mold. The PDMS was cured into an oven at 75°C for 1 hour to crosslink the PDMS. Finally, the PDMS was peeled out of the master mold and cut into the dimensions of the DLD chip.

Three 3 mm holes were punched as inlet reservoirs to hold the blood sample and 1x PBS buffer. A 1.5 mm punch was used in the outlet to connect the device to the tubing and syringe. Finally, the device was bonded onto a glass slide using oxygen plasma surface activation and bonding. The chip was ready to be used the next day.

5.3 Reagents

The beads used were size calibration standards kit 6.2, 7.2, 8.3 and 10.2 μm beads from Bangslab (Bangs Laboratories, Fishers, Indiana). They were resuspended (2 million mL^{-1}) to

be used in the characterisation tests. Lipopolysaccharides from *Escherichia coli* O111:B4 (L2630) and Phorbol 12-myristate 13-acetate (P8139) were purchased from Merck-Sigma (St Louis, Missouri). The LPS concentration (5ng/mL) was determined based on previous works by Segre *et al.*[30] 1x phosphate buffer solutions were used for all dilutions of beads and as sample buffer.

5.4 Donor selection criteria

Patient recruitment from the ED of the National University Hospital, Singapore, was conducted with ethics approval from the local institutional review board (National Healthcare Group Singapore, Domain Specific Review Board, DSRB reference number: 2018/00115). Written informed consent was obtained from enrolled participants.

The ED controls in our study comprised of patients who attended the ED for symptoms unrelated to inflammatory or infectious conditions such as corneal foreign body, poorly controlled hypertension while the healthy volunteers included fellow colleagues working in the ED. These two groups of donors constitute the "no infection" group (Infection Class = 0).

For the "infection" group (Infection Class = 1), we enrolled patients who had a clear and objective source of systemic infection based on preliminary investigations such as chest radiography, urine or blood investigations and fulfils at least 2 SIRS criteria (fever >38 or <36 degrees Celsius; respiratory rate >20/min; heart rate >90/min; white blood cell count > 12,000/mm³, < 4,000/mm³, or > 10% bands).

Vulnerable population (such as pregnant or incarcerated individuals), patients less than 21 years old, those who refused or were unable to provide written informed consent and patients with "do-not-resuscitate" orders were excluded. Additionally, patients with medical conditions or medications that may result in macrocytosis were also excluded as this could potentially interfere with evaluation of WBC size and deformability. These include

conditions such as vitamin B12 deficiency, primary bone marrow disorder, previous gastrectomy, pernicious anemia, alcoholism, COPD, familial macrocytosis, hypothyroidism, cancer and medications like chemotherapy agents, zidovudine, trimethoprim, phenytoin and oral contraceptive pills.

5.5 Blood collection and testing

All blood collected were from venous blood draw with consent from patients at the ED of National University Hospital, Singapore. Post-recruitment, the blood (3 mL) was drawn into a 3 mL EDTA tube and stored in a cooler box to maintain the temperature. The transport of blood from draw to laboratory experiments was within 1 hour. Blood samples (100 µL) was aliquoted out for each test.

5.6 Activation of leukocytes

All WBC experiments, if not tested immediately, were placed on 37°C water bath to ensure physiological conditions. There were no dilutions of blood. LPS activation test (5 ng/mL) was incubated for 30 mins. As each test run was 15 mins, more vials were prepared in time spacing of 3 mins each for testing of each flow rate. This was to ensure the tests were performed at 30 mins interval and the data acquisition time was not a factor. For PMA activation (100nM and 1000nM), the samples were incubated for 2 hours. All sample predilutions were made on 1x PBS.

5.7 Data acquisition and analysis

A Phantom V7.1 (Vision Research, Wayne, New Jersey) was used to capture all visual data from input, output and single cell motion within all DLD devices. The video files were exported into uncompressed ".avi" format for downstream analyses and counting. For each experiment, we captured a total of 2500 frames for analysis. The frame rates used for capture were 15, 30, 60 and 150 fps for 2.5, 5.0, 10.0 and 25.0 µL/min flow rates, respectively. The

analysis of cell counting to plot the histogram was performed by a custom python code, which plots the counted cells against the sub-channel location. From the normalized frequency distribution histogram, the mean, S.D., skew, Kurtosis, frequency, and distribution data were available.

5.8 Machine Classification

Hierarchical clustering and PCA analysis were all performed using python 3.6 with module "scikit-learn". To develop the ROC curve, we used our custom algorithm shown in Figure S13 coupled with support vector machine (SVM) classification using radial basis function kernel. The algorithm used to calculate diagnostic probability values of each sample are shown in Figure S13. Each sample is selected as a "blind" sample and the remaining (n=84) samples are randomly split 9:1 part for boot strapping method of 1000 cycles to validate the prediction of the "blind" sample based on SVM classification. The boot strapping method results in a probability value of predicting the class of "blind" sample. The probability would then be fed into the ROC curve and comparing with its known class for sensitivity and specificity calculation.

5.9 Flow coupled cell simulations

Deformable 2D cell simulations were carried out with the help of a bespoke lattice-Boltzmann-immersed-boundary code. The algorithm is well established for particulate flows in the low Reynolds number regime. The 2D cell is modelled as a ring of marker points that deform according to well defined physical energy potentials. Detailed discussion of methods and results can be viewed in Supplementary Methods 1, Supplementary Table S6, Supplementary Discussion 2.

27

Author Contributions

K.K.Z. and J.H. designed and fabricated the DLD devices. K.K.Z., W.S.K. and J.H. designed the clinical experiments. R.V., G.S. and T.K. developed numerical models for DLD and performed the simulations. W.S.K and M.T.C. applied for IRB and oversaw the clinical trials. W.S.K., M.T.C. and K.Y.Q recruited the patients. K.K.Z and K.Y.Q performed the DLD experiments and data processing. K.K.Z. performed the machine classification and analysis.

Conflict of Interest

No conflict of interest.

Acknowledgement

5

Author Manuscript

References

[1]   K. E. Rudd, S. C. Johnson, K. M. Agesa, K. A. Shackelford, D. Tsoi, D. R. Kievlan, D. V. Colombara, K. S. Ikuta, N. Kissoon, S. Finfer, C. Fleischmann-Struzek, F. R. Machado, K. K. Reinhart, K. Rowan, C. W. Seymour, R. S. Watson, T. E. West, F. Marinho, S. I. Hay, R. Lozano, A. D. Lopez, D. C. Angus, C. J. L. Murray, M. Naghavi, *Lancet.* **2020,** *395* (10219), 200.

[2]   J. Cohen, J. L. Vincent, N. K. Adhikari, F. R. Machado, D. C. Angus, T. Calandra, K. Jaton, S. Giulieri, J. Delaloye, S. Opal, K. Tracey, T. van der Poll, E. Pelfrene, *Lancet Infect. Dis.* **2015,** *15* (5), 581.

[3]   A. McGinley, R. M. Pearse, *BMJ [Br. Med. J.].* **2012,** *345*, e5310.

[4]   D. Wang, B. Hu, C. Hu, F. Zhu, X. Liu, J. Zhang, B. Wang, H. Xiang, Z. Cheng, Y. Xiong, Y. Zhao, Y. Li, X. Wang, Z. Peng, *JAMA.* **2020,** *323* (11), 1061.

[5]   F. Zhou, T. Yu, R. Du, G. Fan, Y. Liu, Z. Liu, J. Xiang, Y. Wang, B. Song, X. Gu, L. Guan, Y. Wei, H. Li, X. Wu, J. Xu, S. Tu, Y. Zhang, H. Chen, B. Cao, *Lancet.* **2020,** *395* (10229), 1054.

[6]   J. S. Boomer, J. M. Green, R. S. Hotchkiss, *Virulence.* **2014,** *5* (1), 45.

[7]   P. H. C. Leliefeld, L. Koenderman, J. Pillay, *Front. Immunol.* **2015,** *6*, 471.

[8]   D. M. Maslove, H. R. Wong, *Trends Mol. Med.* **2014,** *20* (4), 204.

[9]   E. Landhuis, *Nature.* **2018,** *557* (7706), 595.

[10]   A. Oussalah, J. Ferrand, P. Filhine-Tresarrieu, N. Aissa, I. Aimone-Gastin, F. Namour, M. Garcia, A. Lozniewski, J.-L. Guéant, *Medicine.* **2015,** *94* (44), e1774.

[11]   K. Reinhart, M. Bauer, N. C. Riedemann, C. S. Hartog, *Clin. Microbiol. Rev.* **2012,** *25* (4), 609.

[12]   B. Jundi, H. Ryu, D.-H. Lee, R.-E. E. Abdulnour, B. D. Engstrom, M. G. Duvall, A. Higuera, M. Pinilla-Vera, M. E. Benson, J. Lee, N. Krishnamoorthy, R. M. Baron, J. Han, J. Voldman, B. D. Levy, *Nat. Biomed. Eng.* **2019**.

[13]   F. Ellett, J. Jorgensen, A. L. Marand, Y. M. Liu, M. M. Martinez, V. Sein, K. L. Butler, J. Lee, D. Irimia, *Nat. Biomed. Eng.* **2018,** *2* (4), 207.

[14]   N. Toepfner, C. Herold, O. Otto, P. Rosendahl, A. Jacobi, M. Kräter, J. Stächele, L. Menschner, M. Herbig, L. Ciuffreda, L. Ranford-Cartwright, M. Grzybek, Ü. Coskun, E. Reithuber, G. Garriss, P. Mellroth, B. Henriques-Normark, N. Tregay, M. Suttorp, M. Bornhäuser, E. R. Chilvers, R. Berner, J. Guck, *eLife.* **2018,** *7*, 29213.

[15]   C. M. Pitsillides, J. M. Runnels, J. A. Spencer, L. Zhi, M. X. Wu, C. P. Lin, *Cytometry, Part A.* **2011,** *79* (10), 758.

[16]   J. Vuorte, S. E. Jansson, H. Repo, *Cytometry.* **2001,** *43* (4), 290.

[17]   Q. Pan, L. Ye, Z. Deng, L. Li, H. Liu, *J. Immunoassay Immunochem.* **2014,** *35* (4), 368.

[18]   K. K. Zeming, T. Salafi, S. Shikha, Y. Zhang, *Nat. Commun.* **2018,** *9* (1), 1254.

[19]   B. H. Wunsch, J. T. Smith, S. M. Gifford, C. Wang, M. Brink, R. L. Bruce, R. H. Austin, G. Stolovitzky, Y. Astier, *Nat. Nano.* **2016,** *advance online publication*.

[20]   L. R. Huang, E. C. Cox, R. H. Austin, J. C. Sturm, *Science.* **2004,** *304* (5673), 987.

[21]   K. K. Zeming, S. Ranjan, Y. Zhang, *Nat. Commun.* **2013,** *4*, 1625.

[22]   D. W. Inglis, M. Lord, R. E. Nordon, *J. Micromech. Microeng.* **2011,** *21* (5), 054024.

[23]   D. Holmes, G. Whyte, J. Bailey, N. Vergara-Irigaray, A. Ekpenyong, J. Guck, T. Duke, *Interface focus.* **2014,** *4* (6), 20140011.

[24]   F. Fachin, P. Spuhler, J. M. Martel-Foley, J. F. Edd, T. A. Barber, J. Walsh, M. Karabacak, V. Pai, M. Yu, K. Smith, H. Hwang, J. Yang, S. Shah, R. Yarmush, L. V. Sequist, S. L. Stott, S. Maheswaran, D. A. Haber, R. Kapur, M. Toner, *Sci. Rep.* **2017,** *7* (1), 10936.
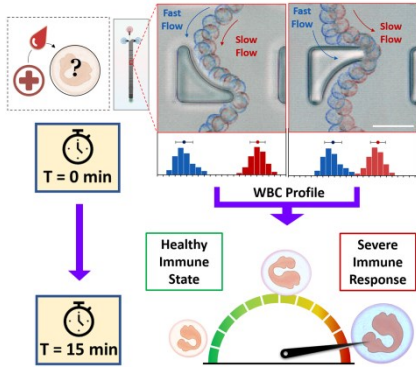
[25]   M. Xavier, S. H. Holm, J. P. Beech, D. Spencer, J. O. Tegenfeldt, R. O. C. Oreffo, H. Morgan, *Lab on a Chip.* **2019,** *19* (3), 513.

[26]   J. T. Smith, B. H. Wunsch, N. Dogra, M. E. Ahsen, K. Lee, K. K. Yadav, R. Weil, M. A. Pereira, J. V. Patel, E. A. Duch, J. M. Papalia, M. F. Lofaro, M. Gupta, A. K. Tewari, C. Cordon-Cardo, G. Stolovitzky, S. M. Gifford, *Lab on a Chip.* **2018,** *18* (24), 3913.

[27]   R. C. Bone, R. A. Balk, F. B. Cerra, R. P. Dellinger, A. M. Fein, W. A. Knaus, R. M. Schein, W. J. Sibbald, *Chest.* **1992,** *101* (6), 1644.

[28]   J. A. Davis, D. W. Inglis, K. J. Morton, D. A. Lawrence, L. R. Huang, S. Y. Chou, J. C. Sturm, R. H. Austin, *Proc. Natl. Acad. Sci. U. S. A.* **2006,** *103* (40), 14779.

[29]   S. Ranjan, K. K. Zeming, R. Jureen, D. Fisher, Y. Zhang, *Lab on a Chip.* **2014,** *14* (21), 4250.

[30]   E. Segre, J. N. Fullerton, *Shock.* **2016,** *45* (5), 490.

[31]   M. Tempel, G. Isenberg, E. Sackmann, *Phys. Rev. E: Stat. Phys., Plasmas, Fluids, Relat. Interdiscip. Top.* **1996,** *54* (2), 1802.

[32]   M. L. Gardel, K. E. Kasza, C. P. Brangwynne, J. Liu, D. A. Weitz, *Methods Cell Biol.* **2008,** *89*, 487.

[33]   E. Spedden, D. L. Kaplan, C. Staii, *Phys. Biol.* **2013,** *10* (5), 056002.

[34]   C. Gabbutt, W. Shen, J. Seifert, S. Contera, *Sci. Reps.* **2019,** *9* (1), 19473.

[35]   K. Crawford, A. DeWitt, S. Brierre, T. Caffery, T. Jagneaux, C. Thomas, M. Macdonald, H. Tse, A. Shah, D. D. Carlo, H. R. O'Neal, *Am. J. Respir. Crit. Care Med.* **2018,** *198* (2), 280.

[36]   W. A. Muller, *Vet. Pathol.* **2013,** *50* (1), 7.

[37]   V. C. Hecht, L. B. Sullivan, R. J. Kimmerling, D.-H. Kim, A. M. Hosios, M. A. Stockslager, M. M. Stevens, J. H. Kang, D. Wirtz, M. G. Vander Heiden, S. R. Manalis, *J. Cell. Biol.* **2016,** *212* (4), 439.

[38]   D. B. Kuhns, D. L. Fink, U. Choi, C. Sweeney, K. Lau, D. L. Priel, D. Riva, L. Mendez, G. Uzel, A. F. Freeman, K. N. Olivier, V. L. Anderson, R. Currens, V. Mackley, A. Kang, M. Al-Adeli, E. Mace, J. S. Orange, E. Kang, S. J. Lockett, D. Chen, P. J. Steinbach, A. P. Hsu, K. A. Zarember, H. L. Malech, J. I. Gallin, S. M. Holland, *Blood.* **2016,** *128* (17), 2135.

[39]   M. Webster, K. L. Witkin, O. Cohen-Fix, *J. Cell Sci.* **2009,** *122* (10), 1477.

[40]   M. K. Brunialti, E. G. Kallás, M. Freudenberg, C. Galanos, R. Salomao, *Cytometry.* **2002,** *50* (1), 14.

[41]   D. R. Gossett, H. T. K. Tse, S. A. Lee, Y. Ying, A. G. Lindgren, O. O. Yang, J. Rao, A. T. Clark, D. Di Carlo, *Proc. Natl. Acad. Sci. U. S. A.* **2012,** *109* (20), 7630.

[42]   M. Herbig, M. Kräter, K. Plak, P. Müller, J. Guck, O. Otto, *Methods Mol. Biol.* **2018,** *1678*, 347.

[43]   K. R. Bashant, A. Vassallo, C. Herold, R. Berner, L. Menschner, J. Subburayalu, M. J. Kaplan, C. Summers, J. Guck, E. R. Chilvers, N. Toepfner, *J. Leukocyte Biol.* **2019,** *105* (6), 1143.

[44]   E. H. A. Spaeny-Dekking, W. L. Hanna, A. M. Wolbink, P. C. Wever, A. J. Kummer, A. J. G. Swaak, J. M. Middeldorp, H. G. Huisman, C. J. Froelich, C. E. Hack, *J. Immunol.* **1998,** *160* (7), 3610.

[45]   E. D. Crouser, J. E. Parrillo, C. Seymour, D. C. Angus, K. Bicking, L. Tejidor, R. Magari, D. Careaga, J. Williams, D. R. Closser, M. Samoszuk, L. Herren, E. Robart, F. Chaves, *Chest.* **2017,** *152* (3), 518.

Author Manuscript

Table of Content Text

A 15-minute label-free immune profiling assay using deterministic lateral displacement (DLD) microfluidics to measure the immune biophysical signatures of cell size and deformability from a drop of whole blood. The assay detects severe immune response of admission patients in the emergency department and the speed of patient stratification has promising impact in deployable point-of-care systems for clinical triage.

5